


ORIGINAL ARTICLE

Optimal design of experiments to improve the characterisation of atrazine degradation pathways in soil

Luciana Chavez Rodriguez¹  | Ana González-Nicolás² | Brian Ingalls³ | Thilo Streck¹ | Wolfgang Nowak² | Sinan Xiao² | Holger Pagel¹

¹Biogeophysics Section, Institute of Soil Science and Land Evaluation, University of Hohenheim, Stuttgart, Germany

²Department of Stochastic Simulation and Safety Research for Hydrosystems (IWS/LS3), University of Stuttgart, Stuttgart, Germany

³Department of Applied Mathematics, University of Waterloo, Waterloo, Ontario, Canada

Correspondence

Luciana Chavez Rodriguez and Holger Pagel, Biogeophysics Section, Institute of Soil Science and Land Evaluation, University of Hohenheim, Stuttgart, 70599, Germany.

Email: l.chavezrodriguez@uni-hohenheim.de (L.C.R.) and

Email: holgerp@uni-hohenheim.de (H.P.)

Funding information

Canadian Natural Sciences and Engineering Research Council (NSERC); Ellrichshausen Foundation; Collaborative Research Centre 1253 CAMPOS, Grant/Award Number: DFG Grant Agreement SFB 1253/1 2017; Research Training Group, Grant/Award Number: RTG 1829; German Research Foundation (DFG)

Abstract

Contamination of soils with pesticides and their metabolites is a global environmental threat. Deciphering the complex process chains involved in pesticide degradation is a prerequisite for finding effective solution strategies. This study applies prospective optimal design (OD) of experiments to identify laboratory sampling strategies that allow model-based discrimination of atrazine (AT) degradation pathways. We simulated virtual AT degradation experiments with a first-order model that reflects a simple reaction chain of complete AT degradation. We added a set of Monod-based model variants that consider more complex AT degradation pathways. Then, we applied an extended constraint-based parameter search algorithm that produces Monte-Carlo ensembles of realistic model outputs, in line with published experimental data. Differences between-model ensembles were quantified with Bayesian model analysis using an energy distance metric. AT degradation pathways following first-order reaction chains could be clearly distinguished from those predicted with Monod-based models. As expected, including measurements of specific bacterial guilds improved model discrimination further. However, experimental designs considering measurements of AT metabolites were most informative, highlighting that environmental fate studies should prioritise measuring metabolites for elucidating active AT degradation pathways in soils. Our results suggest that applying model-based prospective OD will maximise knowledge gains on soil systems from laboratory and field experiments.

Highlights

- Bayesian model analysis can help to distinguish the active degradation pathway of pesticides.
- Information on degradation metabolites is crucial to understand pesticide fate.
- Measurements of specific guilds improve the distinction of active pesticide pathways.
- Prospective optimal design maximizes information gain in soil sciences.

This is an open access article under the terms of the Creative Commons Attribution License, which permits use, distribution and reproduction in any medium, provided the original work is properly cited.

© 2021 The Authors. *European Journal of Soil Science* published by John Wiley & Sons Ltd on behalf of British Society of Soil Science.

KEYWORDS

Bayesian analysis, energy distance, equifinality, first-order kinetics, model discrimination, modelling, Monod kinetics, process constraints, uncertainty quantification, viable parameter set

1 | INTRODUCTION

Pesticides are important chemicals used globally in agriculture to manage plant stressors such as pests, weeds and diseases (Popp et al., 2013). Due to their potential negative effects on ecosystems (de Albuquerque et al., 2020) and human health (Sánchez et al., 2020), some pesticides have been banned or otherwise restricted. The pesticide atrazine (AT) has been banned in Europe in 2004. However, AT and its metabolites are still found in soils and groundwater in potentially harmful concentrations (Jablonowski et al., 2009; Karlsson et al., 2020; Vonberg et al., 2014). In natural environments, AT undergoes abiotic (López-Muñoz et al., 2011) and biotic (Udikovič-Količ et al., 2012) degradation. Several bacterial guilds have been observed to metabolise AT (as a carbon source (Ehrl et al., 2019; Kundu et al., 2019), nitrogen source (Sharma et al., 2019) or both (Udikovič-Količ et al., 2012), leading to an accumulation of intermediate metabolites. Most commonly, these metabolites are hydroxyatrazine (HY) (Karlsson et al., 2020; Smith et al., 2005; Smith & Crowley, 2006), deisopropylatrazine (DIA) and deethylatrazine (DEA) (Meyer et al., 2014; Ngigi et al., 2012; Zhang et al., 2017). Several different (and possibly simultaneously occurring) AT degradation pathways can lead to the formation of identical metabolites. This poses a challenge to the determination of the fate of AT, which in turn confounds our ability to understand why AT persists in natural systems, thus hampering strategies for mitigating pesticide contamination of soils (Chow et al., 2020).

Mathematical modelling approaches are valuable tools for investigating complex degradation pathways such as AT degradation. They provide means for combining the current understanding of AT degradation with mathematical formulations, which can be validated with real measurement data such as AT and metabolite concentrations and biomass (Arhonditsis et al., 2008). In the particular case of AT degradation, the limitation of “which intermediate metabolites and bacterial guilds involved are measured” could lead to distinct mathematical models that all represent the same system with equivalent accuracy (equifinality problem) (Mélykúti et al., 2010). Distinguishing among these competing models can help us to determine which AT degradation pathways are active in a particular environment.

When addressing competing models, two cases arise. If all model formulations predict similar behaviour for all

system elements (AT degradation, metabolite dissipation and biomass formation), then the simplest (most parsimonious) model formulation is usually accepted as the best (most valid) representation. Otherwise, it is important to know which observations may provide the most useful information to distinguish the models and to facilitate *model discrimination* (Chen & Asprey, 2003; Ehrl et al., 2019; Kremling et al., 2004). By identifying relative differences between models, we can reduce the number of competing models, cluster together those that are most similar and facilitate model invalidation (Ehrl et al., 2019; Kremling et al., 2004).

Optimal design (OD) of experiments is a promising tool for addressing the equifinality problem. OD aims to maximise the benefit obtained from experiments (Nowak & Guthke, 2016). If it is done prior to the execution of the experiment, it is called prospective OD (Diggle & Lophaven, 2006; Nowak & Guthke, 2016). In our case, we use prospective OD to identify experimental designs that maximise the observed difference between competing models of AT degradation (Mélykúti et al., 2010). Among multiple metrics used to distinguish models (Chen & Asprey, 2003; Ehrl et al., 2019; Kremling et al., 2004), the concept of energy distance (ED) (Székely & Rizzo, 2013) is a computationally efficient and robust model-distance metric. In this context, the design that produces data with maximised (model to model) ED is considered the OD for model discrimination.

This work applies a prospective OD approach and analyses the trade-off between model complexity and prediction uncertainty to identify modelling approaches that effectively represent AT degradation pathways in soil. We aimed at finding optimal experimental sampling designs and chemical analysis strategies for model discrimination and hence inference of active degradation processes.

2 | MATERIAL AND METHODS

2.1 | AT degradation models

2.1.1 | Conceptual model

We consider a set of hierarchical, nested models for degradation of AT in soils (Figure 1), including biotic and

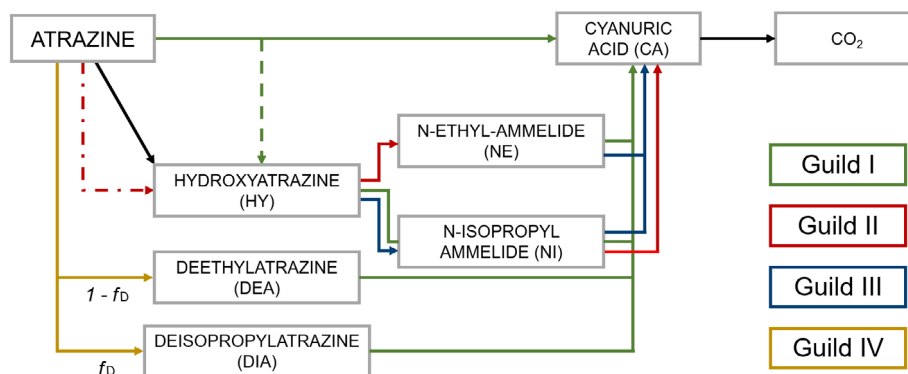


FIGURE 1 Atrazine (AT) degradation in soils: Model framework describing AT, its intermediate metabolites (HY, DEA, DIA, NI, NE and CA), CO₂ and the bacterial guilds involved in the degradation process. Arrow colours indicate guild activity. Black arrows represent abiotic hydrolysis of AT and nitrogen-dependent degradation of CA. The dashed line represents a leak of HY during the degradation process carried out by guild I (Ehrl et al., 2019; Kundu et al., 2019). The dash-dotted line shows a degradation step uncoupled from growth carried out by guild II. The parameter f_D represents the fraction of DIA formed during AT degradation by guild IV. All bacterial guilds respire the metabolites, contributing to CO₂ (not shown in the figure). CA, cyanuric acid; DEA, deethylatrazine; DIA, deisopropylatrazine; HY, hydroxyatrazine; NE, *N*-ethylammelide; NI, *N*-isopropylammelide

abiotic degradation, representing common degradation pathways of AT. These models vary in complexity from a complete Monod model version (M1) to a simple first-order decay model (M6). The latter is commonly used to model degradation at field scale (Bekins et al., 1998).

We assume that degradation processes occur in a well-mixed soil environment that contains a collection of bacterial guilds. These guilds are labelled I, II, III and IV (Figure 1 and Section 2.1.2). Members of each guild are able to fully or partially metabolise bioavailable AT and its intermediate metabolites as sole carbon and energy sources (Deutch et al., 2018; Dutta et al., 2016; Kumar & Singh, 2016) (Figure 1). Nitrogen use is not considered. The members of each guild are partitioned into two sub-pools with different physiological states: active and dormant. Activation and deactivation rates are driven by carbon availability in the system. We explicitly account for a dissolved organic carbon pool (DOC) that serves as a collector of dead cells. The last metabolite of the AT transformation is cyanuric acid (CA) (Zhang et al., 2011). The transformation of CA to carbon dioxide (CO₂) is regulated by nitrogen availability. At high nitrogen concentrations, CA transformation is strongly inhibited by all guilds (García-González et al., 2005).

2.1.2 | Bacterial guilds

We defined four guilds as follows, based on genetic information regarding known AT degraders:

1. Guild I is able to use the side chains of AT as carbon source, degrading it to CA (Dutta et al., 2016; García-

González et al., 2005). Additionally, this guild can use the metabolites HY, NE, NI and the products of the dealkylation of AT (DIA and DEA) as carbon sources (Kolekar et al., 2014). Members of this guild constitutively express a range of functional gene combinations: *atzABC*, *trzN-atzBC* and/or *trzN-atzC* (Ehrl et al., 2019; Kundu et al., 2019). Examples of members of this guild are *Arthrobacter aurescens* TC1 (Ma et al., 2017), and *Ensifer* sp. (Ma et al., 2017).

2. Guild II is able to dechlorinate AT to HY (without gaining either carbon or energy) through the activity of functional genes *atzA* (Smith & Crowley, 2006) or *trzN* (Smith et al., 2005). Additionally, they degrade HY to *N*-ethylammelide (NE) (Smith et al., 2005) (via uncharacterised enzymes), or degrade the metabolite *N*-isopropylammelide (NI) to CA, via the gene *atzC*. An example member of this guild is *Nocardia* sp. (Smith et al., 2005).
3. Guild III uses HY and NI as main carbon and energy sources by harbouring the functional genes *atzB* and *atzC*, yielding CA (Smith et al., 2005; Smith & Crowley, 2006). The *atzC* gene also allows for metabolism of NE as carbon source (Fan & Song, 2014). An example member of this guild is *Rhizobium* sp. (Smith et al., 2005).
4. Guild IV dealkylates AT to the metabolites DEA and DIA in a fixed proportion f_D (Shapir & Mandelbaum, 1997) (Figure 1). Specific genes for this pathway have not been identified; it is most probably a cometabolic process (Huang et al., 2007; Huang et al., 2018) mediated by the unspecific enzyme cytochrome P450 (Meyer et al., 2014). An example member of this guild is *Rhodococcus* sp. (Meyer et al., 2014).

2.1.3 | Process formulations

The models are formulated as ordinary differential equation systems as shown in the Appendix S1, section 1. The rate expressions provided below are general formulations applicable to all models.

1. AT and metabolite dynamics: Together, AT and the intermediate metabolites HY, DEA, DIA, NI and NE are represented by a total carbon concentration C^T , expressed in mass of carbon, segregated into a bioavailable pool (concentration C^L [mg cm^{-3}]), and a sorbed pool (concentration C^S [mg g^{-1}):

$$C^T = \theta \cdot C^L + \rho \cdot C^S, \quad (1)$$

where θ [–] and ρ [g cm^{-3}] are the soil water content and bulk density, respectively.

These two pools are related by the Freundlich isotherm (Freundlich, 1907) with a retardation factor (RF):

$$\text{RF} := 1 + \frac{\rho}{\theta} \cdot K_F^C \cdot n_F^C \cdot (C^L)^{(n_F^C - 1)}, \quad (2)$$

where K_F^C [$\text{mg}^{(1-n_F^C)} \text{g}^{-1} \text{cm}^{n_F^C}$] is the Freundlich coefficient and n_F^C [–] is the Freundlich exponent.

Bioavailable carbon sources (C^L) are taken up and degraded biotically by active guild populations $B_{a,k}$ [mg g^{-1}], where $k = \text{I, II, III or IV}$. We account for two possible fates of consumed substrates: metabolite formation and bacterial metabolism. A fraction $1 - f_C$ of the carbon is converted to the downstream metabolite:

$$r_{\text{metabolite formation}}^{k,C} = \frac{\mu_{k,C} \cdot B_{a,k} \cdot (1 - f_C) \cdot \frac{\rho}{\theta}}{\text{RF}}, \quad (3)$$

where $\mu_{k,C}$ is the growth coefficient (Equation 11), k represents the bacterial guilds, and r is used to express the different metabolic rates.

The remaining fraction f_C contributes to biomass accumulation and to respiration (Equation 18), with yield factor $Y_{k,C}$ [–]:

$$r_{\text{C use}}^{k,C} = \frac{\mu_{k,C} \cdot B_{a,k} \cdot \left(\frac{f_C}{Y_{k,C}} \right) \cdot \frac{\rho}{\theta}}{\text{RF}}. \quad (4)$$

Together, these give an overall uptake rate:

$$r_{\text{uptake}}^{k,C} = \frac{\mu_{k,C} \cdot B_{a,k} \cdot \left(\frac{f_C}{Y_{k,C}} + (1 - f_C) \right) \cdot \frac{\rho}{\theta}}{\text{RF}}. \quad (5)$$

Specific degradation processes that do not involve biomass accumulation and respiration are described as follows:

- Abiotic transformation of AT to HY (photodegradation) has been observed (Kiss & Virág, 2009). We model this process (black arrow in Figure 1) by first-order decay:

$$r_{\text{abiotic degradation}}^{\text{AT}} = \frac{K_o \cdot \text{AT}^L}{\text{RF}}, \quad (6)$$

where K_o [d^{-1}] is the first-order rate coefficient.

- It has been observed that HY leaks out of guild I members by passive diffusion (Ehrl et al., 2019; Kundu et al., 2019) to the soil solution. We modelled this leak flux as a constant fraction of the AT that has been uptaken by guild I:

$$r_{\text{leak}}^{\text{AT-HY}} = \frac{r_{\text{metabolite formation}}^{\text{I,AT}} \cdot f_H}{\text{RF}} \quad (7)$$

where f_H [–] is the fraction of the uptake AT flux that leaks out.

- Guild II dechlorinates AT to HY without gaining carbon or energy (Kundu et al., 2019). We modelled this process with Michaelis–Menten kinetics; this step is not coupled to growth (Dashed-point line in Figure 1):

$$r_{\text{dechlorination}}^{\text{II}} = \frac{k_{\text{AT-HY}} \cdot \text{AT}^L \cdot B_{\text{II,a}} \cdot \frac{\rho}{\theta}}{K_{\text{AT-HY}} + \text{AT}^L \cdot \text{RF}}, \quad (8)$$

where $k_{\text{AT-HY}}$ [d^{-1}] is the dechlorination rate for Guild II, and $K_{\text{AT-HY}}$ [mg cm^{-3}] is the half-saturation concentration.

- Guild IV metabolises AT to DIA and to DEA simultaneously (Meyer et al., 2014). A fraction f_D of the converted AT is in the form of DIA, while the remaining fraction $(1 - f_D)$ is in the form of DEA (Figure 1).
- CA degradation: CA is the final metabolite of AT transformation considered in the model because the further breakdown of CA is typically fast, without accumulation of intermediate metabolites (Aukema et al., 2020; Zhang et al., 2011). The model reflects CA degradation as inhibitory first-order decay:

$$r_{\text{CA-CO}_2} = \frac{\text{CA}^L \cdot d_{\text{CA-CO}_2} \cdot \frac{K_{\text{in}}}{\text{NO}_3 + K_{\text{in}}}}{\text{RF}}, \quad (9)$$

where the $d_{\text{CA-CO}_2}$ [d^{-1}] is the rate of degradation of CA to CO_2 , K_{in} [mg cm^{-3}] is the inhibition factor, and

NO_3 [mg cm^{-3}] is the nitrogen concentration in the system taken as a model parameter.

- Bacterial dynamics and physiology: We describe two subpopulations of all bacterial guilds ($k = \text{I, II, III, IV}$) according to their physiological state: active $B_{k,a}$ or dormant $B_{k,d}$ [mg g^{-1}]. For each guild k , the active population grows at rate r_{growth}^k [$\text{mg g}^{-1} \text{d}^{-1}$] on multiple carbon sources modelled with Monod kinetics allowing for competition for binding sites (Pagel et al., 2014):

$$r_{\text{growth}}^{k,C} = \left(\sum_{C \in C_k} \mu_{k,C} \cdot f_C \right) \cdot B_{k,a} \quad (10)$$

where $C_{\text{I}} = \{\text{AT, HY, DEA, DIA, NE, NI}\}$, $C_{\text{II}} = \{\text{AT, HY, NI}\}$, $C_{\text{III}} = \{\text{HY, NE, NI}\}$, $C_{\text{IV}} = \{\text{AT}\}$ are the potential carbon sources available for the corresponding guilds (specific carbon sources depending on the degradation scenarios are listed in Appendix S1, section 1) and $\mu_{k,C}$ is the growth coefficient defined as:

$$\mu_{k,C} = \frac{\mu_{\text{max}}^{k,C} \cdot C^L}{\mu_{\text{max}}^{k,C} + \mu_{C_k}}, \quad (11)$$

where $\mu_{\text{max}}^{k,C}$ [d^{-1}] is the maximum growth rate for guild k on the available fraction of the carbon source C^L . Function μ_{C_k} is defined as:

$$\mu_{C_k} = \sum_{C \in C_k} (C^L + K_{k,C}), \quad (12)$$

where $K_{k,C}$ [mg cm^{-3}] is the half-saturation concentration of each guild k on each carbon source C^L .

Dormant populations do not grow. Transitions between dormant and active states are described by a switch-like function proposed by Stolpovsky et al. (2011):

$$r_{\text{activation}}^k = \tau_k \cdot k_{k,a} \cdot B_{k,d}, \quad (13)$$

$$r_{\text{deactivation}}^k = (1 - \tau_k) \cdot k_{k,d} \cdot B_{k,a}, \quad (14)$$

where $k_{k,a}$ and $k_{k,d}$ [d^{-1}] are the activation and deactivation coefficients for guild k . Function τ_k is defined as:

$$\tau_k = \left[\exp \left(\frac{C_{\text{th}}^k - \sum_{C \in C_k} C^L}{s \cdot C_{\text{th}}^k} \right) + 1 \right]^{-1}, \quad (15)$$

where C_{th}^k [mg cm^{-3}] is the threshold concentration for the guild k , and s [-] is the steepness parameter set to

0.1 (Mellage et al., 2015).

Both active and dormant subpopulations are subject to linear decay at rate:

$$r_{\text{decay}}^{j,k} = a_{j,k} \cdot B_{k,j}, \quad (16)$$

where $a_{j,k}$ [d^{-1}] is the decay rate coefficient for the guild k and index j represents active or dormant bacterial state.

- DOC formation and bacterial respiration: We included two sink pools:

a. DOC pool which collects dead cells from all guilds ($r_{\text{decay}}^{j,k}$). A fraction f_R of the DOC contributes to the CO_2 pool:

$$r_{\text{DOC}-\text{CO}_2} = r_{\text{decay}}^{j,k} \cdot f_R. \quad (17)$$

b. CO_2 [mg g^{-1}] accumulates due to bacterial respiration at rate:

$$r_{\text{respiration}}^k = \mu_{k,C} \cdot B_{k,a} \cdot f_C \cdot \left(\frac{1 - Y_{k,C}}{Y_{k,C}} \right). \quad (18)$$

2.1.4 | Degradation scenarios

AT is commonly found in soils together with three principal intermediate metabolites HY, DIA and DEA (Kolekar et al., 2019; Krutz et al., 2008; la Cecilia & Maggi, 2017). The additional intermediate metabolites NE and NI are also part of some reported degradation pathways (Smith et al., 2005; Smith & Crowley, 2006), but their accumulation has rarely been reported in soils (Udikoviç-Koliç et al., 2012). Therefore, we considered six degradation scenarios based on the presence or absence of the main bacterial guilds involved in AT degradation. These six

TABLE 1 Degradation scenarios of AT degradation in soils

Model variants	Bacterial guilds	Resulting chemical pools (C)
M1	I, II, III, IV	AT, HY, DIA, DEA, NI, NE
M2	II, III, IV	AT, HY, DIA, DEA, NI, NE
M3	I, III, IV	AT, HY, DIA, DEA, NI
M4	I, II, IV	AT, HY, DIA, DEA, NE
M5	I, IV	AT, HY, DIA, DEA
M6	-	AT, HY, DIA, DEA

Abbreviations: AT, atrazine; DIA, deisopropylatrazine; DEA, deethylatrazine; HY, hydroxyatrazine; NI, *N*-isopropylammelide; NE, *N*-ethyl-ammelide.

scenarios are designed so that the metabolites HY, DIA and DEA are always present (Figure 1 and Table 1). While the first five scenarios yield comparatively complex models (M1–M5 sorted by decreasing complexity), the sixth one (M6) is a simple first-order decay model. This last one only includes the chemical pools AT, HY, DIA, DEA and CA and CO₂. Specific degradation pathways mediated by fungi (Henn et al., 2020) were not considered.

2.2 | Prospective OD of experiments

2.2.1 | Model outputs and generation of simulated data

As model outputs that correspond to candidates for being measured in lab experiments, we considered the concentrations of AT and the metabolites HY, DIA, DEA, NI, NE, CA and CO₂. Additionally, we considered the

TABLE 2 Model parameters for Monod and first-order kinetic models

Parameter	Description	Units	Parameter value	
			Min.	Max.
Monod parameters				
$\mu_{\max}^{k,C}$	Maximal specific growth rate of pesticide degraders	[d ⁻¹]	10 ⁻³	10 ³
$K_{k,C}$	Growth substrate affinity coefficient of pesticide degraders	[mg cm ⁻³]	10 ⁻³	10 ⁵
$k_{k,a}$	Coefficient rate of activation	[d ⁻¹]	10 ⁻⁵	100
$k_{k,d}$	Coefficient rate of deactivation	[d ⁻¹]	10 ⁻⁵	100
C_{th}^k	Threshold concentration	[mg cm ⁻³]	10 ⁻⁶	10 ⁴
$a_{a,k}$	Specific death rate of active bacteria	[d ⁻¹]	10 ⁻³	10 ⁴
$a_{i,k}$	Specific death rate of inactive bacteria	[d ⁻¹]	10 ⁻⁶	10 ⁻²
$Y_{k,C}$	Yield parameter	[-]	0.1	1
k_{AT-HY}	Dechlorination rate	[d ⁻¹]	10 ⁻⁴	10 ³
K_{AT-HY}	Saturation concentration	[mg cm ⁻³]	10 ⁻⁵	10 ⁴
Sorption parameters				
K_F^C	Freundlich coefficient	[mg ^(1-n_F^C) g ⁻¹ cm ^(3n_F^C)]	0.5	10
n_F^C	Freundlich exponent	[-]	0.6	1
First-order decay parameters				
K_o	Abiotic transformation of Atrazine to HY	[d ⁻¹]	10 ⁻⁴	10 ⁵
K_{in}	Inhibition factor	[mg cm ⁻³]	10 ⁻⁴	10 ³
NO ₃	Nitrogen concentration	[mg cm ⁻³]	10 ⁻³	10 ³
d_{AT-HY}	Decay rate of AT to HY	[d ⁻¹]	10 ⁻⁴	10 ³
d_{AT-DD}	Decay rate of AT to DD	[d ⁻¹]	10 ⁻⁴	10 ³
d_{HY-CA}	Decay rate of HY to CA	[d ⁻¹]	10 ⁻⁴	10 ³
d_{DIA-CA}	Decay rate of DIA to CA	[d ⁻¹]	10 ⁻⁴	10 ³
d_{DEA-CA}	Decay rate of DEA to CA	[d ⁻¹]	10 ⁻⁴	10 ³
d_{CA-CO_2}	Decay rate of CA to CO ₂	[d ⁻¹]	10 ⁻⁴	10 ³
Constant rate parameters				
f_R	Fraction of dead bacteria which goes to DOC	[-]	0.01	1
f_H	Leak flux constant	[-]	0.01	1
f_D	Fraction of AT used for DEA formation used by guild D	[-]	0.25	0.75

biomass of the bacterial guild D (the only guild present in all Monod-based model variants), and the total biomass (of all guilds present in the given system formulation).

Our prospective OD analysis is based on simulated data from Monte-Carlo simulations of all models. We chose an initial elevated AT concentration of 100 mg kg^{-1} (Cao et al., 2021; Strong et al., 2002) and a very low initial biomass of AT-degrading bacteria of 0.001 mg kg^{-1} (which represents between 0.001% and 0.0001% of the typical total soil microbial biomass as described by Joergensen (1996) for model simulations, equally divided among the guilds present in the system formulation. We set all bacterial guilds to be dormant and all intermediate metabolites to zero at the beginning of the experiment. To restrict to plausible simulations, we defined a set of parameter and process constraints on the model parameters and outputs based on expert knowledge and soil observations.

The parameter constraints are:

1. Each parameter value must lie in a plausible interval (see Table 2).
2. For each guild, the maximum growth rate coefficient ($\mu_{\max}^{k,C}$) must be higher than the death rate coefficient of active bacteria ($a_{a,k}$).
3. The Freundlich sorption coefficient of HY must be higher than the Freundlich sorption coefficients of AT, DIA, DEA, CA, NI and NE (Abate & Masini, 2005).
4. The Freundlich sorption coefficient of AT must be higher than the Freundlich sorption coefficients of AT, DEA, CA, NE (Abate & Masini, 2005).

The process constraints are:

5. The time taken for 50% of AT to degrade (DT_{50}) (European Food Safety Authority, 2014; FOCUS, 2011) must be between 5 and 25 days (Krutz et al., 2009; Udiković-Kolić et al., 2012).
6. The minimum AT concentration must be at least $10^{-8} \text{ mg ml}^{-1}$ (Vonberg et al., 2014) at the end of the experiment.
7. The mineralisation of initially added AT must be between 20%–80% at the end of the experiment.
8. The DT_{50} of HY, DIA and DEA must be between 2 and 30 days.

These constraints restrict values of the model parameters, either directly (plausible intervals) or indirectly via the interaction of parameters in the process.

2.2.2 | Constraint-based parameter sampling with Markov chain Monte Carlo

The parameter space of the AT biodegradation models is high dimensional (20–70 parameters). Consequently, uniform sampling from the plausible ranges is an inefficient strategy for identifying parameter sets that satisfy the

constraints listed above (Zamora-Sillero et al., 2011). We, therefore, adopted a constraint-based search (CBS) method (Gharari et al., 2014) and modified it to randomly select parameter sets from the viable parameter set. The CBS method is based on an iterative algorithm that applies successively stricter conditions by increasing the minimum acceptable number of process constraints to be satisfied in each iteration. We replaced the original parameter sampling procedure of Gharari et al. (2014) with a Metropolis-Hastings algorithm using a Markov Chain Monte Carlo (MCMC) sampler. This novel CBS-MCMC method (Figure 2) estimates posterior parameter distributions conditional on the defined constraints. In contrast to the original parameter sampling procedure of Gharari et al. (Gharari et al., 2014), MCMC sampling achieves reproducible and unbiased estimates of the viable parameter set (Au, 2004; Hastings, 1970; van Ravenzwaaij et al., 2018).

The CBS-MCMC method consists of the following steps (repeated for each degradation scenario, M1–M6):

1. Define the initial acceptable minimum number of process constraints, n_{\min}^{pc} , beyond the parameter constraint number 1 for the initial sampling (here, $n_{\min}^{\text{pc}} = 2$).
2. Perform an initial Latin hypercube sampling to draw n_{init}^x random parameter sets (here, $n_{\text{init}}^x = 500,000$) using uniform marginal parameter distributions according to the parameter constraint number 1 (see Table 2 for ranges).
3. Accept all parameter sets that satisfy the remaining parameter constraints (2–4). These are called the candidate parameter set (\mathbf{x}_c).
4. Run the current scenario model with each of the candidate parameter sets \mathbf{x}_c and determine the number of process constraints satisfied ($n_{\text{sat}}^{\text{pc}}$) in each case.
5. Accept the parameter sets (\mathbf{x}'_c) resulting in model runs where $n_{\text{sat}}^{\text{pc}} \geq n_{\min}^{\text{pc}}$. Reject all other parameter sets in \mathbf{x}_c .
6. Increase n_{\min}^{pc} by one.
7. Randomly choose n_{MC}^x parameter sets from \mathbf{x}'_c to be used as starting parameter sets (\mathbf{x}_s) in the following steps.
8. Apply the following Metropolis-Hastings algorithm (Au, 2004) with n_{MC}^x parallel Markov chains ($n_{\text{MC}}^x = 40$ in this study):
 - a. Generate new n_{MC}^x candidate parameter sets \mathbf{x}_c^* by randomly modifying values of individual parameters within each parameter set in \mathbf{x}_s using Gaussian jumping distributions. Each jumping distribution is centred at the selected individual parameter value within each parameter set in \mathbf{x}_s and has a standard deviation determined as the standard deviation of the corresponding parameter values in \mathbf{x}'_c . Any parameter values generated

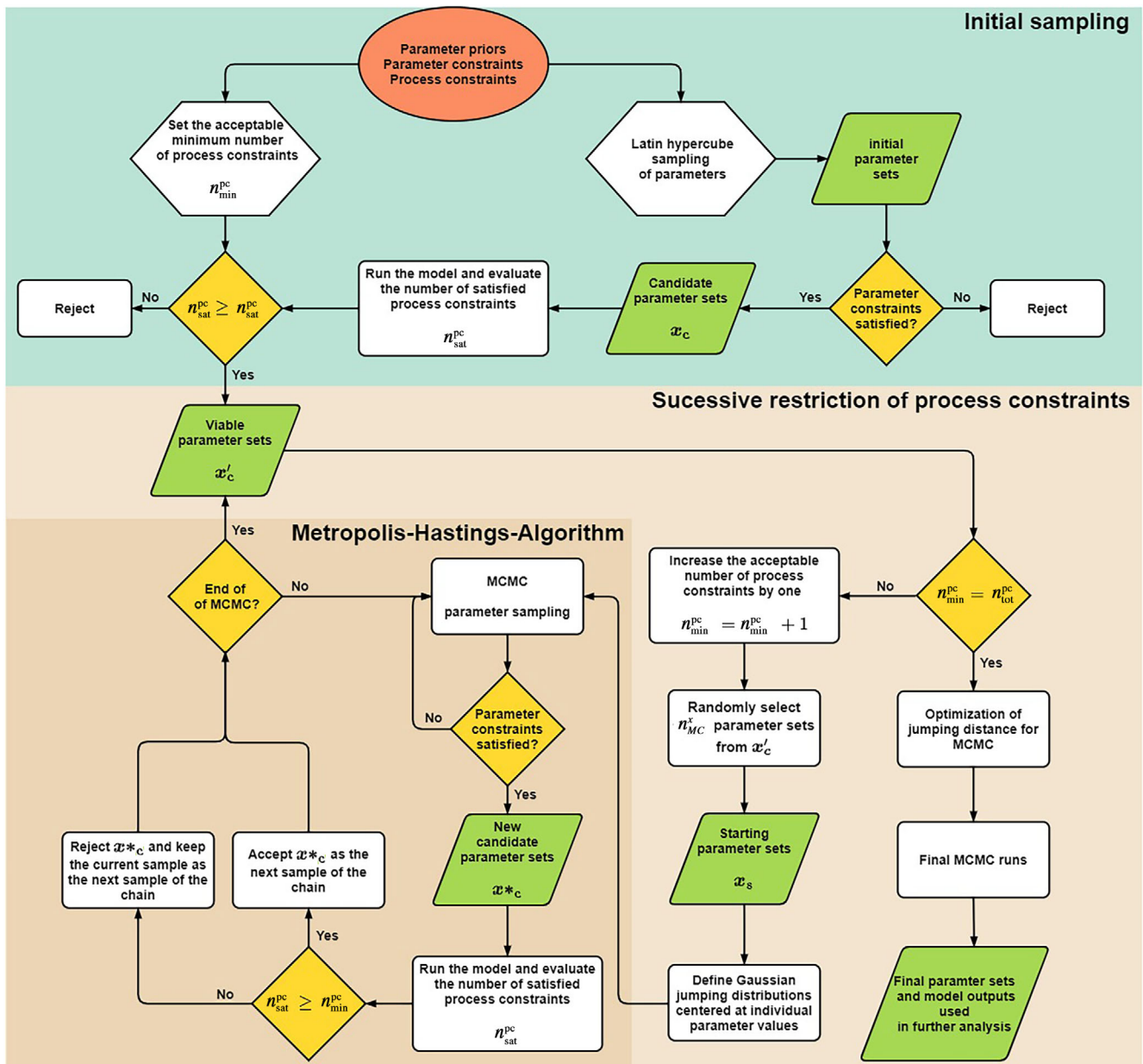


FIGURE 2 Constraint-based search-Markov Chain Monte Carlo method description flowchart

- by the chain that lie outside of parameter constraint 1 (Table 2) are reflected back at the corresponding boundary (Vrugt, 2016). At each step, verify whether the parameter constraints (2–4) are fulfilled. If so, accept the parameter set as a member of the \mathbf{x}_c^* parameters.
- Run the model with each parameter set in \mathbf{x}_c^* and evaluate the number of process constraints satisfied ($n_{\text{sat}}^{\text{pc}}$).
 - Replace \mathbf{x}_s by the corresponding \mathbf{x}_c^* for which $n_{\text{sat}}^{\text{pc}} \geq n_{\text{min}}^{\text{pc}}$. Store \mathbf{x}_c^* in \mathbf{x}_c^l .
 - Repeat 8a to c until termination of the Markov chain (see below).

- Repeat steps 6, 7 and 8 until the $n_{\text{min}}^{\text{pc}}$ equals the total number of process constraints ($n_{\text{tot}}^{\text{pc}}$) and all process constraints are satisfied.
- Optimise the MCMC Gaussian jumping distance (see below) to achieve a desirable acceptance rate.
- Use the tuned MCMC to generate unique model outputs and parameter sets for further analysis.

In step 8, the length of individual Markov chains (l_{MC}) was set to 1000 draws of candidate parameter sets until $n_{\text{min}}^{\text{pc}}$ reached $n_{\text{tot}}^{\text{pc}}$. In the final MCMC runs (Figure 2, bottom left and step 11), l_{MC} is initially set to 5000. If fewer than n_{MC}^x new candidates \mathbf{x}_c^* are accepted in the first run,

l_{MC} is incremented by 5000 and the runs are repeated. As a pre-step for these final MCMC runs, initial runs were performed to tune the acceptance rate of the Metropolis-Hastings algorithm, as follows. We iteratively reduced or increased the standard deviation of the Gaussian jumping distance (division or multiplication by a factor of 1.3) to achieve an acceptance rate of approximately 0.2–0.5 (step 10). The tuned MCMC algorithm was used to generate 30,000 unique model outputs per model for further analysis.

2.2.3 | Bayesian model discrimination with ED

We used the ED as a measure of model dissimilarity. Generically, ED provides a measure of distance between probability distributions (Székely & Rizzo, 2013). For our analysis, we generated distributions of normalised model outputs for particular experimental designs. We used the ED to measure the between-model variability of considered outputs in relation to their within-model variability (Székely & Rizzo, 2013).

$$ED(X, Y) = \sqrt{2 \cdot E \|X - Y\| - E \|X - X'\| - E \|Y - Y'\|}, \quad (19)$$

where X and Y are distributions of model outputs from two model instances (e.g., M1 and M2), and X' and Y' are separate realisations (independent and identically distributed) of the same models, respectively. The term $E \|X - Y\|$ is the expected Euclidian distance between these distributions, while $E \|X - X'\|$ and $E \|Y - Y'\|$ are their expected within-model distances. By subtracting the within-model distance from the between-model distance, we ensure that noisy outputs that do not differ much between models contribute minimally (or even detract from) the ED measure of model separation.

We used a relative error ($E_{rel}(t)$) to normalise model outputs ($y_{normalized}(t)_{m,l}$): AT, metabolites (HY, DIA, DEA, NE, NI, CA), CO₂ and biomass pools for all the models at each time. $E_{rel}(t)$ was tied to the mean value observed at each time for the whole ensemble of each metabolite and across all models ($n_{mc} = 30,000$ sampled outputs):

$$E_{rel}(t) = \text{frac} \cdot \sqrt{\left(\frac{1}{n_{mod}} \cdot \sum_{m=1}^{n_{mod}} \frac{1}{n_{mc}} \cdot \sum_{l=1}^{n_{mc}} y(t)_{m,l} \right)^2}, \quad (20)$$

$$y_{normalized}(t)_{m,l} = \frac{y(t)_{m,l}}{E_{rel}(t)}, \quad (21)$$

where frac is 10%, n_{mod} is the number of models ($n_{mod} = 6$ for analysis including chemicals, $n_{mod} = 5$ for analysis including biomass, and $n_{mod} = 3$ for analyses

including NI and NE metabolites), and n_{mc} is the number of realisations (here, 30,000). This way, observations with larger magnitudes will have larger $E_{rel}(t)$. Due to the normalisation of the model outputs (Equation 21) the scale of ED is such that ED values can be interpreted as a multiple of the standard deviation.

The goal of our prospective OD analysis was to determine those designs (d) that maximise the pairwise ED between the set of models under consideration (Nowak & Guthke, 2016). For pairwise comparison, this amount to:

$$d_{opt} = \underset{d \in D}{\operatorname{argmax}}(ED(M, M')), \quad (22)$$

where D is the set of candidate designs and the $ED(M, M')$ is the pairwise ED between the models M and M' (specified in the Section 3), resulting from any given design d . More generally, we made use of Pareto multi-objective analysis as described below. Each design specifies which of the candidate model outputs are sampled and at what frequency, in a hypothetical lab experiment. The selected output vectors are then substituted as X and Y in Equation (19). To make reliable statements about the ED at acceptable computing time, we chose 10,000 out of the 30,000 simulated data outputs per model variant because this sample size showed a stable ED estimates throughout the candidate designs (Figure S18).

Finally, we normalised the ED scores by the maximum ED of the candidate designs and applied a multi-objective Pareto optimisation (MATLAB's "prtp" function; Polityko, 2021) to determine the non-dominated designs (Deb et al., 2002) (d_{opt}). Here, our OD is multi-objective because the optimisation goal (Equation 22) can be formulated for any pair M, M' of models. In this context, non-dominated designs are better than all other designs in at least one objective. The non-dominated designs are presented as spider plots (Moses, 2021), and were produced in Matlab (see Figures in Sections 3.2 and 3.3).

3 | RESULTS AND DISCUSSION

3.1 | Can we distinguish active AT degradation pathways based on observations of metabolite concentrations?

We explored whether the six proposed models (M1–M6) can be differentiated based on measurements of AT, metabolites (HY, DEA, DIA and CA) and CO₂. Each model variant represents a specific process chain of AT biodegradation and so this model discrimination analysis reveals which of the degradation pathways under consideration can be clearly distinguished based on chemical

data. Because the chemical pools listed above are common to all six model variants (see Figure 1), we considered candidate experimental designs involving measurement of all possible subsets of these pools, a total of 63 possible combinations. We do not impose any resource costs for each measurement channel, and so one might expect that the OD is obvious: measure all chemical pools to maximise the information gathered. However, the ED metric accounts for the trade-off between within-model variability and between-model variability of outputs. Therefore, the inclusion of noisy, information-poor channels results in a *drop* in the ED between models (as demonstrated below). Thus, considering noisy output channels in the experimental design deteriorates model discriminability.

With the 63 possible combinations of chemical output channels, we consider three different sampling frequencies: (i) every day until day 25 (short), (ii) every 2 days until day 50 (mid), (iii) every 4 days until day 100 (long), giving $63 \times 3 = 189$ designs in total (details of the designs are provided in <https://doi.org/10.5281/zenodo.5501948>).

Figure 3 shows pairwise model ED scores for every candidate experimental design. At this stage, deciphering the individual 63 designs is not critical. Based on a minimum ED threshold value of two for model discrimination (horizontal dashed lines in Figure 3), we observed that the models fell into three distinguishable groups: (i) M1, M2, M3 and M4 (henceforth $M|1-4$); (ii) M5; and (iii) the first-order decay model M6. We selected a minimum ED of two because and similarly to standard deviations, a two standard deviation distance would correspond to being outside of the 95% confidence interval.

As expected the simplest, first-order decay model (M6) can be clearly distinguished from the Monod-based models (M1–M5) with all experimental designs, except when only measuring AT (first design in each time-related group) regardless of the sampling frequency (Figure 3a).

Likewise, M5 clustered separately. In M5, the complete AT degradation and dealkylation of AT is mediated by bacterial guilds A and D. There is no formation of NI and NE because the microbial guilds B and C are missing. The absence of these two guilds leads to reduced biodegradation of HY. Additionally, the main source of HY in the soil solution is the leak out of guild A (Ehrl et al., 2019; Kundu et al., 2019) or abiotically produced HY (de Paula et al., 2016; Fan & Song, 2014).

Models M1, M3 and M4 clustered within a joint group ($M|1-4$). These three models account for AT dealkylation and dechlorination by guilds A and D, and either guild B or C is present. Interestingly, M2 clusters within the $M|1-4$ group, too, despite the absence of the full degradation pathway of AT carried out by guild A. The absence of guild A eliminates any degradation of the chlorinated AT metabolites DIA, and DEA (Huang

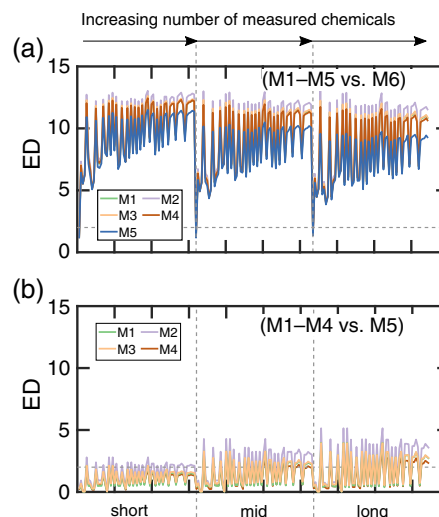


FIGURE 3 Pairwise energy distances (ED) (expressed in standard deviation units) over the candidate designs (details of the designs are provided in <https://doi.org/10.5281/zenodo.5501948>). (a) between M1–M5 and M6, (b) between M1–M4 and M5. Additional combinations are shown in Figure S19. The candidate experimental designs include three sampling frequencies—(i) daily over 25 day (short), (ii) every second day over 50 day (mid) and (iii) every 4 days over 100 days (long)—in combination with a number of one to six measured chemicals. The horizontal line represents the selected minimum ED threshold for model discrimination (distance of two standard deviations). M1 in green is located under the other model lines in both panels

et al., 2018; Huang et al., 2020), leading to the accumulation of both compounds. However, the accumulation of DIA and DEA occurred largely at concentrations below detection and the overall dynamics of AT and its metabolites was comparable to the other models within this group. Models within this group are not distinguishable based on AT, metabolite observations (HY, DIA, and DEA, CA), and CO_2 (Figure S19). Because each model variant within $M|1-4$ represents a specific variant of potentially active AT degradation pathways, additional measurements of microbial biomass might improve model discrimination and thus allow identification of the corresponding active AT degradation pathways, as we discuss below (Section 3.3).

3.2 | Which experimental designs provide the most informative data for model discrimination?

We analysed the discrimination of the three identified model groups in detail by calculating EDs between (i) $M|1-4$ and M6, (ii) M5 and M6, (iii) $M|1-4$ and M5. In this analysis, comparison between M5 and M6 with group $M|1-4$ was done by treating the group

M|1–4 as a single model by adding up the individual EDs from models M1 to M4 (group M|1–4) to M5 and M6 and normalising it by the maximum added ED of the candidate designs. We performed a multi-objective Pareto analysis (see Section 2) to determine the designs that maximise group discrimination, i.e., those experimental designs which lead to a maximum ED of one objective, while simultaneously minimising the ED decrease of the objectives (non-dominated Pareto optimal solutions).

3.2.1 | ODs and measured pools

The analysis revealed the following six Pareto ODs: (i) measurement of DEA, DIA, and CA with short length, (ii) measurement of CA in mid length, (iii) measurement of DEA, DIA and CA with mid length, (iv) measurement of CA in long length, (v) measurement of DIA and CA with long length and (vi) measurement of DEA, DIA and CA with long length. Figure 4 shows that the non-dominated designs in the middle and long schemes are visually almost indistinguishable, meaning they offer the same advantage in differentiating the models, and therefore, we plotted them with the same colour.

None of the six ODs include measurements of AT, HY or CO₂. Thus, these chemical pools do not provide informative data for model discrimination (This result can be suspected from the similarities of their simulated time-series for all degradation scenarios; Figures S12–S17). Including these measurements incorporates noise into the ED measure, confounding model discrimination. For example, as shown in Table 3, addition of the AT output channel increases the noise component of the ED, with negligible increase in the comparison component.

We can, therefore, conclude that to understand the fate of AT in natural systems, one should prioritise information about the intermediate metabolites (DEA, DIA, CA) that populate the design results in Figure 4. Unfortunately, most dissipation experiments on AT to date have mainly measured AT (Briceño et al., 2010; Nousiainen et al., 2014).

CA seems to provide the most informative data among the intermediate metabolites because it is mainly accumulated in all selected ODs (principal end product of AT degradation in our simulations). This well resembles field observations, where further degradation of CA to CO₂ occurs only under low concentrations of nitrogen (N) in soils (Dutta et al., 2016; García-González et al., 2005). Additionally, DIA and DEA, products of the dealkylation of AT (Huang et al., 2007; Kolekar et al., 2014), occur in four of six non-dominated designs. The power of these two pools to enhance model discrimination is expected due to the different DIA and DEA dynamics simulated by the models. For example, DIA and DEA are hardly produced (under the detection limit of 10⁻⁷ mg cm⁻³) by models in Group M1–4. In contrast, M6 and M5 simulate detectable DIA and DEA concentrations (Figures S12–S17), leading to differences in the ED.

The first-order decay model M6 can be better distinguished from the other groups in short-term designs. This can be read from Figure 4-short by realising that the top and right nodes in light green are much closer to the edge than the pink (mid) and green (long) nodes. Clearly, short-term designs measuring CA every day are superior for discrimination of the first-order decay model (M6) from M5 and M|1–4 but are less powerful for discrimination within the Monod models M1 to M5 (Figure 4a). This could be related to the tendency of first-

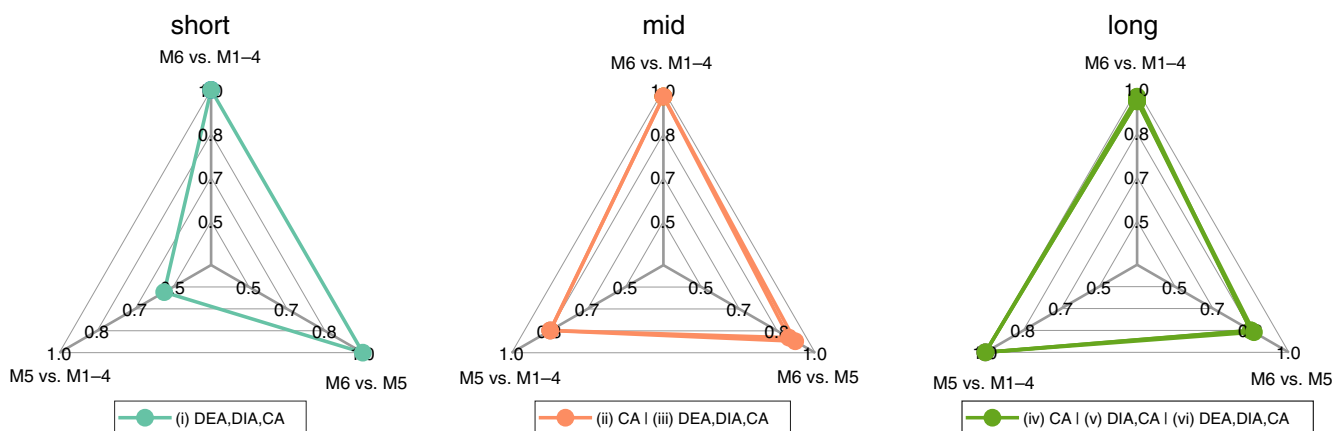


FIGURE 4 Optimal experimental designs based on chemical measurements AT, metabolite (HY, DEA, DIA, CA) and CO₂ for three sampling frequencies (short: Every day sampling until day 25, mid: Every 2 days sampling until day 50, long: Every 4 days sampling until day 100. Axes showed normalised ED values for each objective (see Section 2). AT, atrazine; CA, cyanuric acid; DEA, deethylatrazine; DIA, deisopropylatrazine

TABLE 3 Variability decomposition of the M1–6 ED discriminating between-model M1 (X) and M6 (Y)

AT	DEA	DIA	CA	Time	$2 \cdot E \ X - Y \ $	$-E \ X - X' \ $	$-E \ Y - Y' \ $	$\sqrt{ED(X, Y)}$
N	Y	Y	Y	1	339.1	8.0	171.9	12.6
Y	Y	Y	Y	1	341.5	19.6	173.1	12.2
N	N	N	Y	3	198.6	13.8	35.6	12.2
Y	N	N	Y	3	211.6	38.9	45.5	11.3

Note: Non-dominated designs and equivalent designs, including AT. As expected, by including AT measurements, the increase in noise outweighs the increase in comparison, so that in total, the value of ED decreases.

order decay models to quickly reach steady-state in the simulations. For discriminating the Monod model M5 from the group M|1–4, sampling every 4 days and measuring DEA, DIA and CA is the best option (Figure 4b,c) because these groups produce distinctive endpoints of the metabolites that differ according to the associated pathway.

3.3 | Can measuring pools not commonly measured improve model discrimination?

In the analyses in Sections 3.1 and 3.2, we considered experimental designs that involve measurements of AT, the metabolites (HY, DIA, DEA, CA) and CO₂. These correspond to measurements that could be typically collected in lab dissipation experiments (Krutz et al., 2008). Next, we examine the potential of less typical measurements: biomass and the NI and NE metabolite pools. We begin by defining three new sets of candidate designs additionally incorporating (i) measurements of total biomass and/or biomass of guild D (255 possible combinations of chemicals and biomass and three sampling frequencies giving 765 designs), (ii) the metabolite NI (127 possible combinations of chemicals and three sampling frequencies giving 381 designs) and (iii) the metabolite NE (127 possible combinations of chemicals and three sampling frequencies giving 381 designs). Because models M6 and M5 can already be differentiated based on the chemical measurements, we focused only on distinguishing models within group M|1–4.

3.3.1 | Role of biomass measurements

We observed, that by adding the biomass information, the EDs increased, allowing model discrimination (Figure 5) of all models within group M|1–4. These results highlight the importance of biomass measurements for discriminating the models and the corresponding active AT degradation pathways in soils.

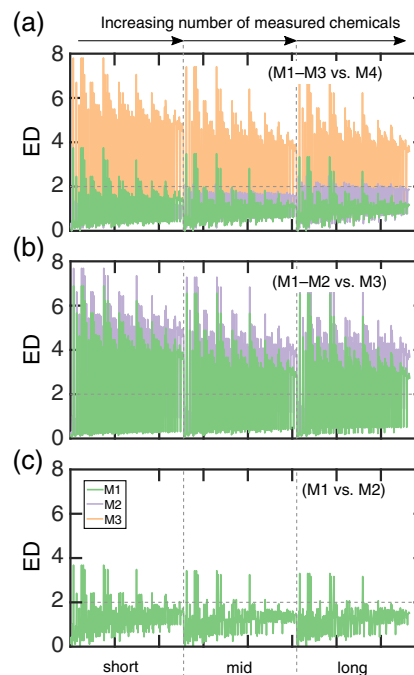


FIGURE 5 Pairwise energy distances (EDs) (expressed in standard deviation units). (a) between M1 and M4, (b) between M1 and M3, (c) between M1 and M2. The candidate experimental designs include three sampling frequencies: daily over 25 days (short), every second day over 50 (mid), every 4 days over 100 (long). Details of the designs are provided in <https://doi.org/10.5281/zenodo.5501948>. The horizontal line represents the selected minimum ED threshold for model discrimination (distance of two standard deviations)

We applied a Pareto analysis to the 765 biomass-including designs to maximise the distance between models in group M|1–4. We identified 15 of the 765 designs as Pareto optimal, shown in Figure 6. Similarly to Figure 4, some of the non-dominated designs are almost indistinguishable to one another, meaning they offer the same advantage in differentiating the models, and have, therefore, been plotted with the same colour. Unsurprisingly, these ODs showed that measurements of total biomass do not contribute to model discrimination. However, also not surprisingly, measurement of guild D biomass helps to distinguish among the Monod models.

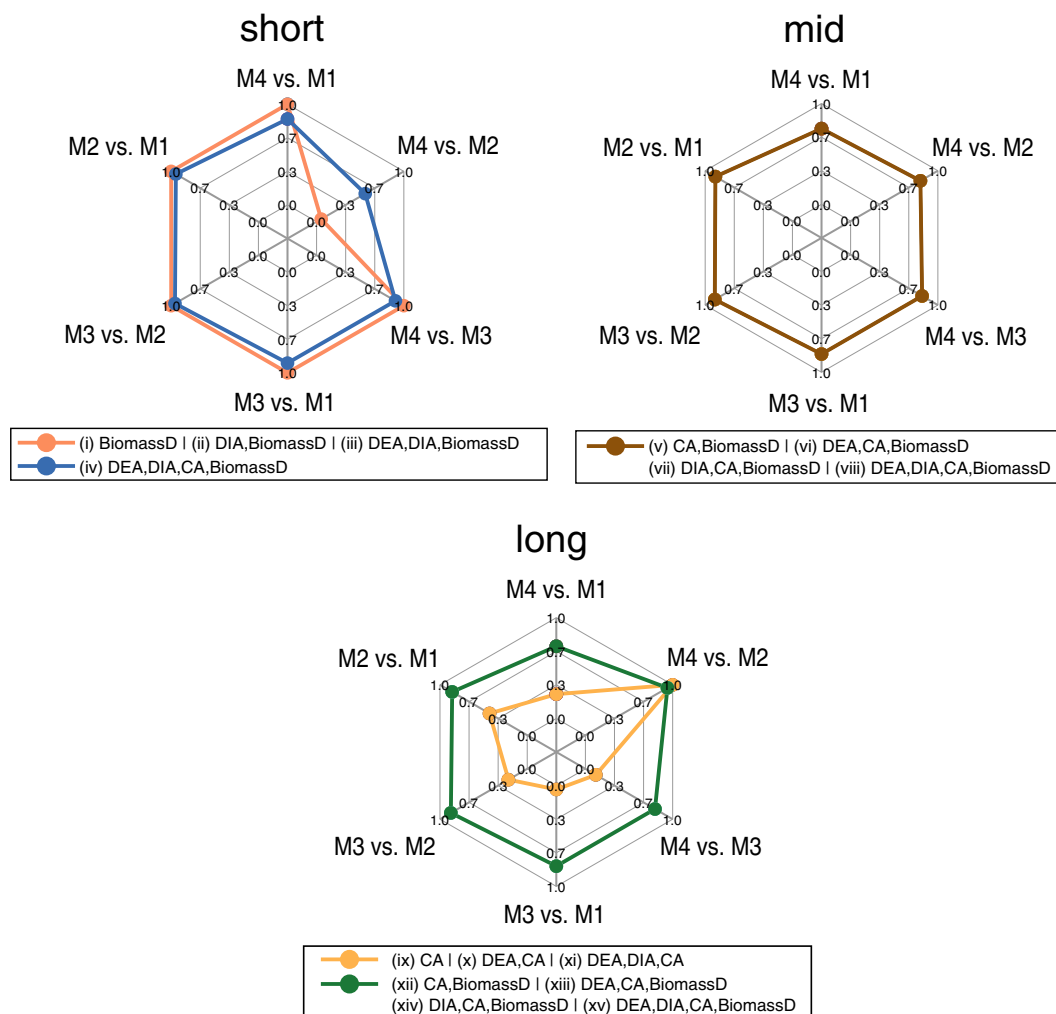


FIGURE 6 Optimal designs (ODs) including biomass measurements (biomass of guild D and total biomass). The candidate experimental designs include three sampling frequencies: Daily over 25 days (short), every second day over 50 (mid), every 4 days over 100 (long). Axes showed normalised ED values for each objective (see Section 2). Designs that are almost identical are painted in the same colour

Unfortunately, distinguishing specific guilds is challenging. Guild membership could be estimated from specific genes responsible for AT degradation, as done by Pagel et al. (2016) for the herbicide MCPA. However, some degraders contain genes from multiple guilds, leading to an overestimation of the degrader biomass. We expect that advances in molecular biology will provide the tools to make a more accurate quantitative identification of particular degraders, and thus, pathway identification possible.

A closer look at the optimal experimental designs reveals that “short” experiments including biomass of guild D and the metabolite CA improve the identification of models M2 and M4 with a minor impact on the ED of the other pair of models (Figure 6). Similar results are observed in “mid” experimental designs (Figure 6).

Interestingly, neglecting biomass of guild D in “long” experimental schemes favours only the identification of M2 and M4 and hampers the identification of all the other pairs of models.

3.3.2 | Role of NI and NE measurements

Similar to biomass, NI and NE are not typically measured. Therefore, we explored whether we can enhance active AT pathway discrimination by including them in our experimental designs. Results of pairwise ED for all designs are shown in Figure 7. NI and NE metabolites appear only in models M1, M2, M3 and M1, M2 and M4, respectively. Including NI measurements enables model M3 to be distinguished from models M1 and M2, especially

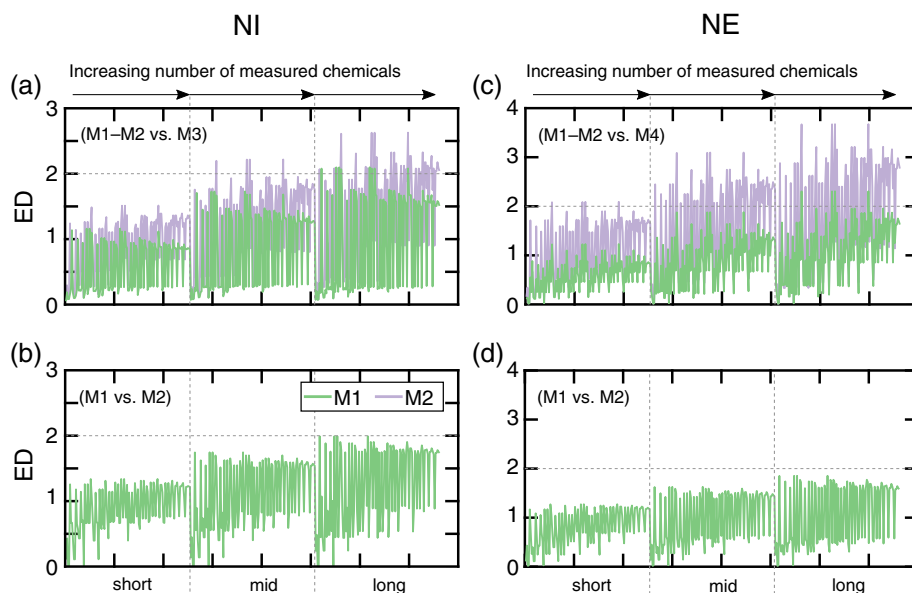


FIGURE 7 Pairwise energy distances (EDs) (expressed in standard deviation units) including (i) NI: (a) between M1 and M3, (b) between M2; and (ii) NE: (c) between M4, and (d) between M2. The candidate experimental designs include three sampling frequencies—(i) daily over 25 days (short), every second day over 50 (mid), every 4 days over 100 (long). Details of the designs are provided in <https://doi.org/10.5281/zenodo.5501948>. The horizontal line represents the selected minimum ED threshold for model discrimination (distance of two standard deviations). NE, *N*-ethylammelide; NI, *N*-isopropylammelide

TABLE 4 Optimal designs after multi-objective pareto analysis of candidate designs including NI and NE in addition to AT, metabolites (HY, DIA, DEA, CA) and CO₂ in long-term schemes

	Designs				ED	
	DEA	DIA	CA	NI	M1–M3	M2–M3
(i)	Y	Y	N	Y	0.4	1
(ii)	Y	Y	Y	Y	1	1
	DEA	DIA	CA	NE	M1–M4	M2–M4
(i)	N	Y	Y	Y	1	1
(ii)	Y	Y	Y	Y	1	1

Abbreviations: AT, atrazine; CA, cyanuric acid; DEA, deethylatrazine; DIA, deisopropylatrazine; HY, hydroxyatrazine; NE, *N*-ethylammelide; NI, *N*-isopropylammelide.

in designs that include mid and long sampling frequencies (Figure 7a). Likewise, including NE measurements enables to differentiate M4 from M1 and M2 (Figure 7c).

Because adding NI and NE metabolites measurements does not contribute to model discrimination between-model M1 and M2 (Figure 7b,d), when applying the multi-objective Pareto analysis to NI- and NE-containing designs, we focused on the following model pairs: (i) M3 versus M1, (ii) M3 versus M2, for the designs including NI; and (i) M4 versus M1, (ii) M4 versus M2 for the designs including NE (381 in each case). A spiderplot with a single pair generates a straight line, and so the results are presented equivalently in Table 4. Two designs (each per row) were determined as the non-dominated designs per analysis (Table 4). CA observations in experimental designs, including NI, enable distinction of M2

from M3, but not of M1 from M3. Additionally, when including NE in the experimental design, DEA measurements do not improve model discrimination between M1, M2 and M4. Thus, these designs including NI and NE measurements can support model discrimination and pathway identification if biomass is not measured. However, these two metabolites are rarely found in soils (De Souza et al., 2000), probably because of relatively fast degradation rates in comparison to the formation of preceding AT metabolites (Krutz et al., 2009). Regarding sampling frequencies and duration of experiments, long experiments (every 4 days sampling until day 100) proved to be more helpful for model discrimination when including NI and NE measurements (Table 4).

4 | CONCLUSIONS

In this work, we applied a prospective OD of experiments to find experimental sampling strategies that allow for discrimination among competing atrazine (AT) degradation models and the corresponding degradation pathways. Our method is reliable (Figure S18), and it can be performed prior to the execution of the experiment. Applying the Bayesian constrained-based parameter search algorithm (CBS-MCMC) for efficiently sampling the viable parameter set dramatically reduced the computational demand. The CBS-MCMC method is widely applicable to other biogeochemical models and provides a powerful tool to leverage expert knowledge for constructing robust prior parameter distributions for model sensitivity analysis or calibration.

We found that the five proposed Monod models could be reduced to two groups, according to their predominant features. Considering the intermediate metabolites (DIA

and DEA), and especially CA is an integral part of understanding the complete degradation pathway of AT and of adequate model selection as well. Measurements of specific pesticide degrader biomass or molecular proxies such as functional gene abundances provide the information to discriminate models further and identify which specific degradation pathways are active. Thus, experimental measurements of specific guilds should be prioritised in the future.

For a practical application of our results towards the identification of the active AT degradation pathway in soils, we recommend using the following protocol:

1. Include the OD setup in the sampling strategy for the planned experiment, but extend the sampling frequency and the number of measured variables as far as the budget allows. For better model discrimination, the best design should include measurements of specific biomass degraders (examples in Figure 6).
2. Calibrate all available models to all measurements and include the ODs.
3. Leverage the measured OD data to select model structures that best represent the studied system.
4. Identify active process chains based on the selected model structures and exclude processes exclusively considered in invalidated models (Kremling et al., 2004).

The application of prospective OD of experiments requires that models use correct process descriptions. Therefore, the candidate model formulations must be carefully selected to ensure that the best possible representation is used (Nowak & Guthke, 2016). As long as such valid process models are available—as in this study for atrazine degradation—model-based prospective OD will maximise the knowledge gain on soil systems from laboratory and field experiments.

ACKNOWLEDGEMENTS

The authors acknowledge support by the state of Baden-Württemberg through bwHPC. This study was financially supported by the German Research Foundation (DFG) within the Research Training Group “Integrated Hydro-system Modelling” (RTG 1829) and the Collaborative Research Centre 1253 CAMPOS (DFG Grant Agreement SFB 1253/1 2017) as well as by the Ellrichshausen Foundation and the Canadian Natural Sciences and Engineering Research Council (NSERC). Open Access funding enabled and organized by Projekt DEAL.

CONFLICT OF INTEREST

The authors declare that the research was conducted in the absence of any commercial or financial relationships that could be construed as a potential conflict of interest.

DATA AVAILABILITY STATEMENT

The codes that support the findings of this study are available from the corresponding author upon reasonable request. Example codes can be found in <https://doi.org/10.5281/zenodo.5501948>.

AUTHOR CONTRIBUTIONS

Luciana Chavez Rodriguez: Conceptualization (equal); formal analysis (lead); investigation (lead); methodology (equal); software (equal); visualization (lead); writing – original draft (lead); writing – review and editing (equal). **Ana González-Nicolás:** Conceptualization (equal); methodology (equal); software (equal); validation (equal); writing – review and editing (equal). **Brian Ingalls:** Conceptualization (equal); supervision (equal); writing – original draft (supporting); writing – review and editing (equal). **Thilo Streck:** Funding acquisition (lead); project administration (equal); resources (lead); writing – review and editing (equal). **Wolfgang Nowak:** Conceptualization (equal); methodology (equal); project administration (equal); software (equal); writing – review and editing (equal). **Sinan Xiao:** Conceptualization (equal); methodology (equal); validation (equal); writing – review and editing (equal). **Holger Pagel:** Conceptualization (equal); formal analysis (supporting); investigation (supporting); methodology (equal); software (equal); supervision (equal); validation (equal); visualization (supporting); writing – original draft (supporting); review and editing (equal).

ORCID

Luciana Chavez Rodriguez  <https://orcid.org/0000-0003-1510-6695>

REFERENCES

- Abate, G., & Masini, J. C. (2005). Sorption of atrazine, propazine, deethylatrazine, deisopropylatrazine and hydroxyatrazine onto organovermiculite. *Journal of the Brazilian Chemical Society*, 16, 936–943.
- Arhonditsis, G. B., Perhar, G., Zhang, W., Massos, E., Shi, M., & Das, A. (2008). Addressing equifinality and uncertainty in eutrophication models. *Water Resources Research*, 44(1), W01420.
- Au, K. S. (2004). Probabilistic failure analysis by importance sampling Markov chain simulation. *Journal of Engineering Mechanics*, 130(3), 303–311.
- Aukema, K., Tassoulas, L., Robinson, S., Konopatski, J., Bygd, M., & Wackett, L. (2020). Cyanuric acid biodegradation via biuret: Physiology, taxonomy, and geospatial distribution. *Applied and Environmental Microbiology*, 86(2), e01964–19.
- Bekins, B. A., Warren, E., & Godsy, E. M. (1998). A comparison of zero-order, first-order, and Monod biotransformation models. *Ground-Water*, 36(2), 261–268.
- Briceño, G., Jorquera, M. A., Demanet, R., Mora, M. L., Durán, N., & Palma, G. (2010). Effect of cow slurry amendment on atrazine dissipation and bacterial community structure in

- an agricultural Andisol. *Science of the Total Environment*, 408(14), 2833–2839.
- Cao, D., He, S., Li, X., Shi, L., Wang, F., Yu, S., Xu, S., Ju, C., Fang, H., & Yu, Y. (2021). Characterization, genome functional analysis, and detoxification of atrazine by *Arthrobacter* sp. C2. *Chemosphere*, 264, 128514.
- Chen, B. H., & Asprey, S. P. (2003). On the design of optimally informative dynamic experiments for model discrimination in multiresponse nonlinear situations. *Industrial & Engineering Chemistry Research*, 42(7), 1379–1390.
- Chow, R., Scheidegger, R., Doppler, T., Dietzel, A., Fencia, F., & Stamm, C. (2020). A review of long-term pesticide monitoring studies to assess surface water quality trends. *Water Research X*, 9, 100064.
- de Albuquerque, F. P., de Oliveira, J. L., Moschini-Carlos, V., & Fraceto, L. F. (2020). An overview of the potential impacts of atrazine in aquatic environments: Perspectives for tailored solutions based on nanotechnology. *Science of the Total Environment*, 700, 134868.
- de Paula, R. T., de Abreu, A. B. G., de Queiroz, M. E. L. R., Neves, A. A., & da Silva, A. A. (2016 feb). Leaching and persistence of ametryn and atrazine in red-yellow latosol. *Journal of Environmental Science and Health, Part B*, 51(2), 90–95.
- De Souza, M. L., Newcombe, D., Alvey, S., Crowley, D. E., Hay, A., Sadowsky, M. J., & Wackett, L. P. (2000). Molecular basis of a bacterial consortium: Interspecies catabolism of atrazine. *Applied and Environmental Microbiology*, 66(3), 178–184.
- Deb, K., Pratap, A., Agarwal, S., & Meyarivan, T. (2002). A fast and elitist multiobjective genetic algorithm: NSGA-II. *IEEE Transactions on Evolutionary Computation*, 6(2), 182–197.
- Deutch, C. E., Bui, A. P., & Ho, T. (2018). Growth of *Paenarthrobacter aureus* strain TC1 on atrazine and isopropylamine during osmotic stress. *Annals of Microbiology*, 68(9), 569–577.
- Diggle, P., & Lophaven, S. (2006). Bayesian geostatistical design. *Scandinavian Journal of Statistics*, 33(1), 53–64.
- Dutta, A., Vasudevan, V., Nain, L., & Singh, N. (2016). Characterization of bacterial diversity in an atrazine degrading enrichment culture and degradation of atrazine, cyanuric acid and biuret in industrial wastewater. *Journal of Environmental Science and Health, Part B*, 51(1), 24–34.
- Ehrl, B. N., Kundu, K., Gharasoo, M., Marozava, S., & Elsner, M. (2019). Rate-limiting mass transfer in micropollutant degradation revealed by isotope fractionation in chemostat. *Environmental Science & Technology*, 53(3), 1197–1205.
- European Food Safety Authority. (2014). EFSA Guidance Document for evaluating laboratory and held dissipation studies to obtain DegT50 values of active substances of plant protection products and transformation products of these active substances in soil.
- Fan, X., & Song, F. (2014). Bioremediation of atrazine: Recent advances and promises. *Journal of Soils and Sediments*, 14(10), 1727–1737.
- FOCUS (2006). Guidance Document on Estimating Persistence and Degradation Kinetics from Environmental Fate Studies on Pesticides in EU Registration. Report of the FOCUS Work Group on Degradation Kinetics, EC Document Reference Sanco/10058/2005 (version 2.0). 434 pp. Retrieved from https://esdac.jrc.ec.europa.eu/public_path/projects_data/focus/dk/docs/FOCUSkineticsvc1.1Dec2014.pdf
- Freundlich, H. (1907). Über die Adsorption in Lösungen. *Zeitschrift für Physikalische Chemie*, 57U(1), 385–470.
- García-González, V., Govantes, F., Porrúa, O., & Santero, E. (2005). Regulation of the *Pseudomonas* sp. strain ADP cyanuric acid degradation operon. *Journal of Bacteriology*, 187(1), 155–167.
- Gharari, S., Shahei, M., Hrachowitz, M., Kumar, R., Fencia, F., Gupta, H. V., & Savenije, H. H. (2014). A constraint-based search algorithm for parameter identification of environmental models. *Hydrology and Earth System Sciences*, 18(12), 4861–4870.
- Hastings, W. K. (1970). Monte Carlo sampling methods using Markov chains and their applications. *Biometrika*, 57(1), 97–109.
- Henn, C., Monteiro, D. A., Boscolo, M., da Silva, R., & Gomes, E. (2020). Biodegradation of atrazine and ligninolytic enzyme production by basidiomycete strains. *BMC Microbiology*, 20(1), 266.
- Huang, H., Zhang, C., Rong, Q., Li, C., Mao, J., Liu, Y., Chen, J., & Liu, X. (2020). Effect of two organic amendments on atrazine degradation and microorganisms in soil. *Applied Soil Ecology*, 152, 103564.
- Huang, H., Zhang, C., Zhang, P., Cao, M., Xu, G., Wu, H., Zhang, J., Li, C., & Rong, Q. (2018 nov). Effects of biochar amendment on the sorption and degradation of atrazine in different soils. *Soil and Sediment Contamination: An International Journal*, 27(8), 643–657.
- Huang, H., Zhang, S., Xq, S., Chen, B. D., Zhu, Y. G., & Bell, J. N. B. (2007). Effect of arbuscular mycorrhizal fungus (*Glomus caledonium*) on the accumulation and metabolism of atrazine in maize (*Zea mays* L.) and atrazine dissipation in soil. *Environmental Pollution*, 146(2), 452–457.
- Jablonowski, N. D., Köppchen, S., Hofmann, D., Schäffer, A., & Burauel, P. (2009). Persistence of 14C-labeled atrazine and its residues in a field lysimeter soil after 22 years. *Environmental Pollution*, 157, 2126–2131.
- Joergensen, R. G. (1996). The fumigation-extraction method to estimate soil microbial biomass: Calibration of the kEC value. *Soil Biology and Biochemistry*, 28(1), 25–31.
- Karlsson, A. S., Lesch, M., Weihermüller, L., Thiele, B., Disko, U., Hofmann, D., Vereecken, H., & Spielvogel, S. (2020). Pesticide contamination of the upper Elbe River and an adjacent floodplain area. *Journal of Soils and Sediments*, 20(4), 2067–2081.
- Kiss, A., & Virág, D. (2009). Interpretation and modelling of environmental behaviour of diverse pesticides by revealing photodecomposition mechanisms. *Microchemical Journal*, 92(2), 119–122.
- Kolekar, P. D., Patil, S. M., Suryavanshi, M. V., Suryavanshi, S. S., Khandare, R. V., Govindwar, S. P., & Jadhav, J. P. (2019). Microcosm study of atrazine bioremediation by indigenous microorganisms and cytotoxicity of biodegraded metabolites. *Journal of Hazardous Materials*, 374, 66–73.
- Kolekar, P. D., Phugare, S. S., & Jadhav, J. P. (2014). Biodegradation of atrazine by *Rhodococcus* sp. BCH2 to N-isopropylammelide with subsequent assessment of toxicity of biodegraded metabolites. *Environmental Science and Pollution Research International*, 21(3), 2334–2345.
- Kremling, A., Fischer, S., Gadkar, K., Doyle, F. J., Sauter, T., Bullinger, E., Allgöwer, F., & Gilles, E. D. (2004). A benchmark for methods in reverse engineering and model discrimination:

- Problem formulation and solutions. *Genome Research*, 14(9), 1773–1785.
- Krutz, L. J., Burke, I. C., Reddy, K. N., Zablotowicz, R. M., & Price, A. J. (2009). Enhanced atrazine degradation: Evidence for reduced residual weed control and a method for identifying adapted soils and predicting herbicide persistence. *Weed Science*, 57(4), 427–434.
- Krutz, L. J., Shaner, D. L., Accinelli, C., Zablotowicz, R. M., & Henry, W. B. (2008). Atrazine dissipation in s-triazine-adapted and nonadapted soil from Colorado and Mississippi: Implications of enhanced degradation on atrazine fate and transport parameters. *Journal of Environmental Quality*, 37(3), 848–857.
- Kumar, A., & Singh, N. (2016). Atrazine and its metabolites degradation in mineral salts medium and soil using an enrichment culture. *Environmental Monitoring and Assessment*, 188(3), 142.
- Kundu, K., Marozava, S., Ehrl, B., Merl-Pham, J., Griebler, C., & Elsner, M. (2019). Defining lower limits of biodegradation: Atrazine degradation regulated by mass transfer and maintenance demand in *Arthrobacter aurescens* TC1. *The ISME Journal*, 13(9), 2236–2251.
- la Cecilia, D., & Maggi, F. (2017). In-situ atrazine biodegradation dynamics in wheat (*Triticum*) crops under variable hydrologic regime. *Journal of Contaminant Hydrology*, 203, 104–121.
- López-Muñoz, M. J., Aguado, J., & Revilla, A. (2011). Photocatalytic removal of s-triazines: Evaluation of operational parameters. *Catalysis Today*, 161(1), 153–162.
- Ma, L., Chen, S., Yuan, J., Yang, P., Liu, Y., & Stewart, K. (2017). Rapid biodegradation of atrazine by *Ensifer* sp. strain and its degradation genes. *International Biodeterioration & Biodegradation*, 116, 133–140.
- Mellage, A., Eckert, D., Grösbacher, M., Inan, A. Z., Cirpka, O. A., & Griebler, C. (2015). Dynamics of suspended and attached aerobic toluene degraders in small-scale flow-through sediment systems undergrowth and starvation conditions. *Environmental Science and Technology*, 49(12), 7161–7169.
- Mélykúti, B., August, E., Papachristodoulou, A., & El-Samad, H. (2010). Discriminating between rival biochemical network models: Three approaches to optimal experiment design. *BMC Systems Biology*, 4(1), 38.
- Meyer, A. H., Dybala-Defratyka, A., Alaimo, P. J., Geronimo, I., Sanchez, A. D., Cramer, C. J., & Elsner, M. (2014). Cytochrome P450-catalyzed dealkylation of atrazine by *Rhodococcus* sp. strain NI86/21 involves hydrogen atom transfer rather than single electron transfer. *Dalton Transactions*, 43(32), 12175–12186.
- Moses, Y. (2021). Spider plot. https://github.com/NewGuy012/spider_plot.
- Ngigi, A. N., Getenga, Z. M., Boga, H. I., & Ndalut, P. K. (2012). Biodegradation of s-triazine herbicide atrazine by *Enterobacter cloacae* and *Burkholderia cepacia* sp. from long-term treated sugarcane-cultivated soils in Kenya. *Journal of Environmental Science and Health Part B, Pesticides, Food Contaminants, and Agricultural Wastes*, 47(8), 769–778.
- Nousiainen, A. O., Björklöf, K., Sagarkar, S., Mukherjee, S., Purohit, H. J., Kapley, A., & Jørgensen, K. S. (2014). Atrazine degradation in boreal nonagri-cultural subsoil and tropical agricultural soil. *Journal of Soils and Sediments*, 14(6), 1179–1188.
- Nowak, W., & Guthke, A. (2016). Entropy-based experimental design for optimal model discrimination in the geosciences. *Entropy*, 18(11), 409.
- Pagel, H., Ingwersen, J., Poll, C., Kandeler, E., & Streck, T. (2014). Micro-scale modeling of pesticide degradation coupled to carbon turnover in the detritusphere: Model description and sensitivity analysis. *Biogeochemistry*, 117(1), 185–204.
- Pagel, H., Poll, C., Ingwersen, J., Kandeler, E., & Streck, T. (2016). Modeling coupled pesticide degradation and organic matter turnover: From gene abundance to process rates. *Soil Biology and Biochemistry*, 103, 349–364.
- Polityko, E. (2021). Calculation of Pareto points. <https://www.mathworks.com/matlabcentral/fileexchange/22507-calculation-of-pareto-points>.
- Popp, J., Pet, K., & Nagy, J. (2013). Pesticide productivity and food security. A review. *Agronomy for Sustainable Development*, 33, 243–255.
- Sánchez, O. F., Lin, L., Bryan, C. J., Xie, J., Freeman, J. L., & Yuan, C. (2020). Profiling epigenetic changes in human cell line induced by atrazine exposure. *Environmental Pollution*, 258, 113712.
- Shapir, N., & Mandelbaum, R. T. (1997). Atrazine degradation in subsurface soil by indigenous and introduced microorganisms. *Journal of Agricultural and Food Chemistry*, 45(11), 4481–4486.
- Sharma, A., Kalyani, P., Trivedi, V. D., Kapley, A., & Phale, P. S. (2019). Nitrogen-dependent induction of atrazine degradation pathway in *Pseudomonas* sp. strain AKN5. *FEMS Microbiology Letters*, 366(1), fny277.
- Smith, D., Alvey, S., & Crowley, D. E. (2005). Cooperative catabolic pathways within an atrazine-degrading enrichment culture isolated from soil. *FEMS Microbiology Ecology*, 53(2), 265–273.
- Smith, D., & Crowley, D. E. (2006). Contribution of ethylamine degrading bacteria to atrazine degradation in soils. *FEMS Microbiology Ecology*, 58(2), 271–277.
- Stolpovsky, K., Martinez-Lavanchy, P., Heipieper, H. J., Van Cappellen, P., & Thullner, M. (2011). Incorporating dormancy in dynamic microbial community models. *Ecological Modelling*, 222(17), 3092–3102.
- Strong, L. C., Rosendahl, C., Johnson, G., Sadowsky, M. J., & Wackett, L. P. (2002). *Arthrobacter aurescens* TC1 metabolizes diverse s-triazine ring compounds. *Applied and Environmental Microbiology*, 68(12), 5973–5980.
- Székely, G. J., & Rizzo, M. L. (2013). Energy statistics: A class of statistics based on distances. *Journal of Statistical Planning and Inference*, 143(8), 1249–1272.
- Udiković-Kolić, N., Scott, C., & Martin-Laurent, F. (2012). Evolution of atrazine-degrading capabilities in the environment. *Applied Microbiology and Biotechnology*, 96(5), 1175–1189.
- van Ravenzwaaij, D., Cassey, P., & Brown, S. D. (2018). A simple introduction to Markov Chain Monte-Carlo sampling. *Psychonomic Bulletin & Review*, 25(1), 143–154.
- Vonberg, D., Vanderborght, J., Cremer, N., Pütz, T., Herbst, M., & Vereecken, H. (2014). 20 years of long-term atrazine monitoring in a shallow aquifer in western Germany. *Water*, 50, 294–306.
- Vrugt, J. A. (2016). Markov chain Monte Carlo simulation using the DREAM software package: Theory, concepts, and MATLAB implementation. *Environmental Modelling and Software*, 75, 273–316.

- Zamora-Sillero, E., Hafner, M., Ibig, A., Stelling, J., & Wagner, A. (2011). Efficient characterization of high-dimensional parameter spaces for systems biology. *BMC Systems Biology*, *142*(1), 142.
- Zhang, J. J., Gao, S., Xu, J. Y., Lu, Y. C., Lu, F. F., Ma, L. Y., Su, X. N., & Yang, H. (2017). Degrading and phytoextracting atrazine residues in rice (*Oryza sativa*) and growth media intensified by a phase II mechanism modulator. *Environmental Science & Technology*, *51*(19), 11258–11268.
- Zhang, Y., Jiang, Z., Cao, B., Hu, M., Wang, Z., & Dong, X. (2011). Metabolic ability and gene characteristics of *Arthrobacter* sp. strain DNS10, the sole atrazine-degrading strain in a consortium isolated from black soil. *International Biodeterioration & Biodegradation*, *65*(8), 1140–1144.

SUPPORTING INFORMATION

Additional supporting information may be found in the online version of the article at the publisher's website.

How to cite this article: Chavez Rodriguez, L., González-Nicolás, A., Ingalls, B., Streck, T., Nowak, W., Xiao, S., & Pagel, H. (2022). Optimal design of experiments to improve the characterisation of atrazine degradation pathways in soil. *European Journal of Soil Science*, *73*(1), e13211. <https://doi.org/10.1111/ejss.13211>